Waveform-Relocated Earthquake Catalog for Oklahoma and Southern Kansas Illuminates the Regional Fault Network

by Martin Schoenball and William L. Ellsworth

ABSTRACT

For much of Oklahoma, augmentation of the seismic network with new public stations in the activated areas has followed rather than preceded the spread of seismicity across the state, and consequently the network geometry is often unfavorable for resolving the underlying fault structures. With this study, we reanalyze the existing earthquake catalog with additional data from two industry-operated networks for the period May 2013 to November 2016. These networks include 40 seismic stations and cover seismically active north-central Oklahoma with a station spacing on the order of 25 km. Relative locations obtained from waveform cross correlation reveal a striking pattern of seismicity, illuminating many previously unmapped faults. Absolute depths are usually well constrained to within 1 km. Relative locations provide about one order of magnitude better precision for resolving the structure of seismicity clusters. Relocated epicenters tend to cluster in linear trends of less than 1 km to more than 20 km in length. In areas with stations closer than about 10 km, we can resolve fault planes by strike and dip. These are generally in agreement with surface-wave-derived moment-tensor solutions.

Electronic Supplement: Catalog of relocated earthquakes.

INTRODUCTION

Oklahoma and southern Kansas experienced an unprecedented uptick of seismicity in recent years that has been linked to large-scale wastewater disposal into the Arbuckle formation that is overlaying the crystalline basement in the region (Ellsworth, 2013; Walsh and Zoback, 2015; Weingarten *et al.*, 2015). Studying swarms of earthquakes has given us insights into the fluid-related processes that drive natural swarms (Vidale and Shearer, 2006; Chen *et al.*, 2012; Hauksson *et al.*, 2013; Zaliapin and Ben-Zion, 2013; Shelly *et al.*, 2016) and indications about how these processes are different for anthropogenic earthquake swarms (Schoenball *et al.*, 2015; Zaliapin and Ben-Zion, 2016). Although the underlying processes of pore pressure increase leading to reduction of effective stresses are understood at a large scale (Raleigh *et al.*, 1976), the details of these processes in Oklahoma, such as the mechanisms driving individual sequences, are not well understood. This is in part due to the inadequate seismic monitoring during the major uptick of seismicity in that region.

For much of Oklahoma, augmentation of the publicly available seismic network with new stations in the activated areas has followed rather than preceded the spread of seismicity across the state, and consequently the network geometry is often unfavorable for resolving the underlying fault structures. Recently, archived data from company-operated seismic networks were made available to the community, enabling earthquake relocation with much higher precision. The main goal of this study was to harness the additional station coverage provided by two industry-operated seismic networks that became available recently in addition to the public stations. Adding these two networks to the list of queried stations provides a homogeneous station coverage for the study area, with station spacing on the order of 25 km or better beginning in May 2013. This increased coverage provides the basis for a much higher location precision and an effective subsequent relative relocation procedure.

In this article, we describe a catalog of more than 18,000 relocated earthquakes covering the period from May 2013 to November 2016 for the Oklahoma and southern Kansas region. Below, we summarize our relocation procedure, explore the location uncertainties, and discuss some key observations from the relocations.

METHODS

As the basis for this study, we use the earthquake detections and locations from the Oklahoma Geological Survey (OGS) and manually reviewed picks from the National Earthquake Information Center (NEIC) for a subset of these events and for the Kansas earthquakes (see Data and Resources). We initially select events bounded by longitude −99.5° to −96° and latitude 35.2° to 37.5°. For events with published manually reviewed

doi: 10.1785/0220170083

Table 1
Velocity Model, with Alternative Layer Boundaries in Brackets

Layer Top (km)	V_P (km/s)	V_S (km/s)
0	2.70	1.52
0.3	2.95	1.66
1	4.15	2.33
1.5 (1.2, 1.7)	5.80	3.26
8 (7.7, 8.5)	6.27	3.52
21	6.41	3.60

picks available from NEIC, we pick additional *P*- and *S*-phase arrivals for the 40 additional stations of the two privately operated networks (see Data and Resources). For event detections from OGS, no picks are published, and we choose *P*- and *S*-phase arrivals for all stations within 1° of the starting location that were available for download from the Incorporated Research Institutions for Seismology website or among the private data. Data processing was performed using the Python packages ObsPy (Krischer *et al.*, 2015). For automatic picking of *P*- and *S*-phase arrivals, we use the package PhasePApy (Chen and Holland, 2016), which includes an implementation of the Akaike information-criterion picker (Maeda, 1985).

We base our 1D velocity model (Table 1) on the one used by OGS for their routine locations (Darold *et al.*, 2015). The velocity model has layer boundaries at 1.5 and 8 km depth, among others, representing the top of basement and the top of the middle crust, respectively. We create two alternative models in which we shift these boundaries to 1.2 and 7.7 km in variant 1 and to 1.7 and 8.5 km in variant 2, respectively. The original OGS velocity model uses a V_P/V_S ratio of 1.73. However, velocity well logs indicate higher values, especially in the shallower sediments. We use a constant V_P/V_S ratio of 1.78. Final absolute locations were obtained by averaging the locations for the three velocity models.

New absolute locations were obtained using the HYPOINVERSE-2000 program (Klein, 2014). We require picks from at least four stations and use the implemented distance-weighting scheme. Stations closer than 30 km are given full weights, and we reduce the weights to 0 at 60-km distance using a cosine taper (Klein, 2014). Further refinement through relative relocation is done using hypoDD, leveraging the higher precision of differential travel-time measurements (Waldhauser and Ellsworth, 2000). For each earthquake, we store differential times for up to the 20 closest neighboring earthquakes at a maximal distance of 10 km. For each earthquake pair, differential travel times for *P* and *S* phases at up to 20 stations are stored. In total, we compute about 5,000,000 differential travel times. For earthquake pairs that are less than 2 km apart after the initial absolute location, we attempt to compute refined differential travel times using waveform cross correlation. Waveforms are band-pass filtered between 2 and 20 Hz. Subsample precision is achieved following the approach of Deichmann and Garcia-Fernandez (1992) by fitting a parabola through the five samples closest to the sample with the highest cross-correlation coefficient. We perform the cross correlations on all components and measure the differential travel time using the one yielding the highest cross-correlation coefficient. We require a cross-correlation coefficient of at least 0.7 to retain this differential travel-time measurement and use the squared cross-correlation coefficient as its weight in the relocation procedure. About 1,800,000 differential travel times could be computed this way.

In the first iterations of hypoDD, we give the differential times derived from catalog pick times the highest weight to constrain the overall geometry using all earthquakes. In later iterations and for event separations less than 2 km, we fold in differential travel times measured using cross-correlation time lags and decrease the weight of the less-precise catalog picks. In the last step, we use only cross-correlation measurements for events not farther apart than 600 m to resolve the fine structure below that scale. Events that could not be relocated by hypoDD were rejected, and duplicate events in the OGS catalog were deleted.

In the final catalog, we report the same magnitudes that were given by NEIC or OGS. We would like to stress here that cross comparisons of M_L given by both sources indicate a discrepancy of about 0.2 magnitude units, with higher values given by OGS. The magnitude of completeness is about 2.8, and might be about 2.6 if we account for the generally higher-quoted magnitudes by OGS.

RESULTS

The major improvement of our locations stems from data of the additional 40 industry-operated stations that provide an even coverage of the area, with station spacing on the order of 25 km. Additional stations that were installed during our study period primarily improved the depth constraint of earthquake sequences.

Uncertainties

Of the initial 19,342 events, we retained and could relocate 18,578 earthquakes using hypoDD, and for 13,813 of those, we successfully cross correlated waveforms for the highest relocation precision. Location precision determined by HYPOINVERSE-2000 is generally better than 300 m (74% of events) in the horizontal direction, with 90% of events located in the horizontal direction better than 620 m (Fig. 1a,b). In the vertical direction, precisions are generally better than 1000 m (77% of events), with 90% of events located in the vertical direction better than 2.12 km (Fig. 1). Relative location uncertainties vary throughout the study region and are reflected by the fidelity with which structures such as fault planes are delineated by hypocenters. We perform a jackknife analysis of the relocations with 500 resampled subsets of differential times to assess the relative location uncertainty. For each jackknife calculation, we randomly select 90% of differential time measurements and run hypoDD. The errors are then obtained from the

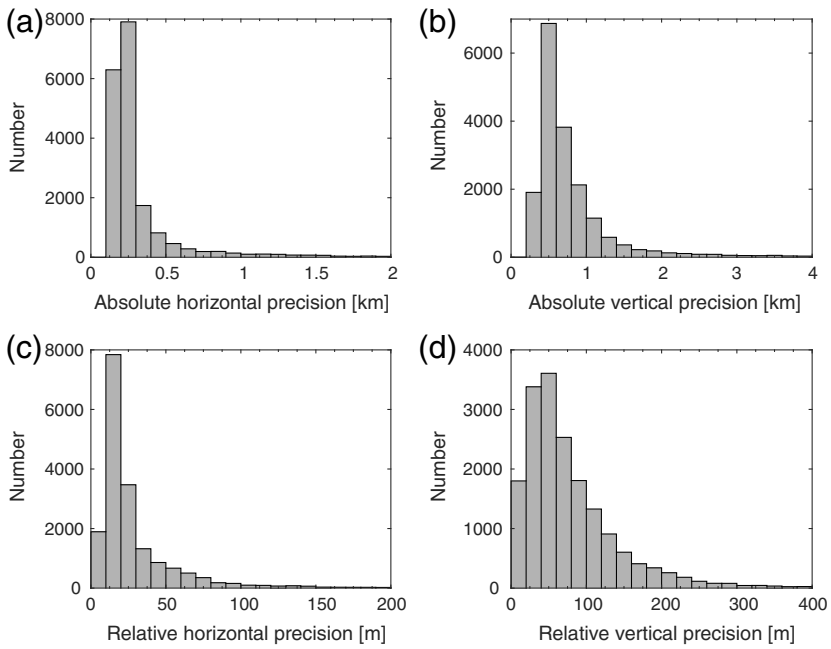

▲ **Figure 1.** Distributions of location precision. (a, b) Location precision given by HYPOINVERSE-2000 in horizontal and vertical directions, respectively. (c, d) Distributions of relative location errors in horizontal and vertical directions, respectively. Relative errors in (c) and (d) were obtained from jackknife tests using hypoDD, for which we randomly remove 10% of the differential time measurements for each of 500 realizations.

covariance matrix of the spatial distribution of resulting hypocenter coordinates. In Figure 1c,d, we show the resulting distributions for the relative uncertainty. Generally, the relative location uncertainty is about one order of magnitude smaller than the absolute location precision. Throughout this article and in the catalog, uncertainties given are at the 1-sigma level.

Fault Structures

Our earthquake relocations sharpen the image of the recent seismicity in the study area. Tight lineations of epicenters clearly outline a network of faults (Fig. 2). We observe a poor agreement of the lineations and the database of known fault traces (Holland, 2015). Only in very few cases do earthquakes align with the trace of a known fault. Importantly, the clear pattern of preferred fault orientations deduced from hypocenters and readily visible in Figure 2 is absent in the fault database. This indicates that there are large-scale structures present in the basement that are not prominently seen in the sedimentary cover from which the fault map was assembled. More importantly, the known fault map provides a biased picture of the present fault system, predominantly representing faults poorly aligned with the stress field and hence unlikely to slip (Walsh and Zoback, 2016). Generally, a very good agreement is observed with the moment-tensor solution obtained from surface-wave modeling described in Herrmann *et al.* (2011) and available online for more-recent earthquakes (Fig. 3a).

Looking at the hypocenters in 3D, we notice that much of the study area can be characterized as a network of predominantly subvertical strike-slip faults. South of Guthrie and north of Medford and into the Kansas portion of the study area, a significant population of normal faults were activated in addition to subvertical strike-slip faults. Halfway between Medford and Enid, there is a remarkable series of at least four subparallel major faults striking east-northeast (ENE; Fig. 3b). Each of these faults was reactivated along about 10 or more kilometers along their strike. Remarkably, despite the extensive reactivation of these faults, the largest earthquake observed here is magnitude 3.9, corresponding to a rupture area about 1 km across. Moment tensors agree with the interpretation that these faults are indeed rupturing along their strike and not as part of a large system of en echelon faults. In the region between Pawnee and Stillwater, we notice three 20–30 km long arcs of relatively scattered seismicity (Fig. 3c). For portions of these arcs, seismicity is more tightly clustered along planes oriented at an angle relative to these arcs. Here, it appears that the arcuate fault zones are indeed formed by an en echelon pattern of smaller faults. However, no moment tensors are available to support this hypothesis.

The very energetic Fairview sequence, with several M 4 earthquakes and one M 5.1 event, overlaps ~3 km of a previously known fault and extends the known fault trace to the northeast (Holland, 2015; Yeck *et al.*, 2016). Our relocations show an intriguing alignment of earthquake epicenters of up to M 3.1 extending to another previously known fault that hosted the 19 November 2015 M 4.7 Cherokee earthquake (Fig. 3d). If indeed all these earthquakes are hosted by the same fault structure, then fault reactivation has occurred along about 48 km of this fault so far. The known segment of this fault extends by another 15 km further ENE into the study area, albeit at an orientation potentially less favorable for slip because it has not been reactivated yet. Although the moment tensors of the Cherokee and Fairview events are consistent with right-lateral strike-slip faulting, we do not have enough information to conclude the same for the connecting events and to be certain that they indeed belong to the same structure.

An interesting example that demonstrates the quality of our catalog is an earthquake cluster between Harper and Anthony, Kansas, at the northern edge of our study area. Two normal fault planes are resolved by the hypocenters (Fig. 4). The first reactivated plane is dipping to southeast. Approximately perpendicular to that fault, a second normal fault was reactivated dipping northwest. Moment tensors show two normal-faulting earthquakes with 45°-dipping nodal planes, corresponding to two M 4.3 and M 3.8 events, respectively, and aligning with the second fault plane (Herrmann *et al.*, 2011). The moment tensors are in excellent agreement with a fault plane outlined by the hypocenters.

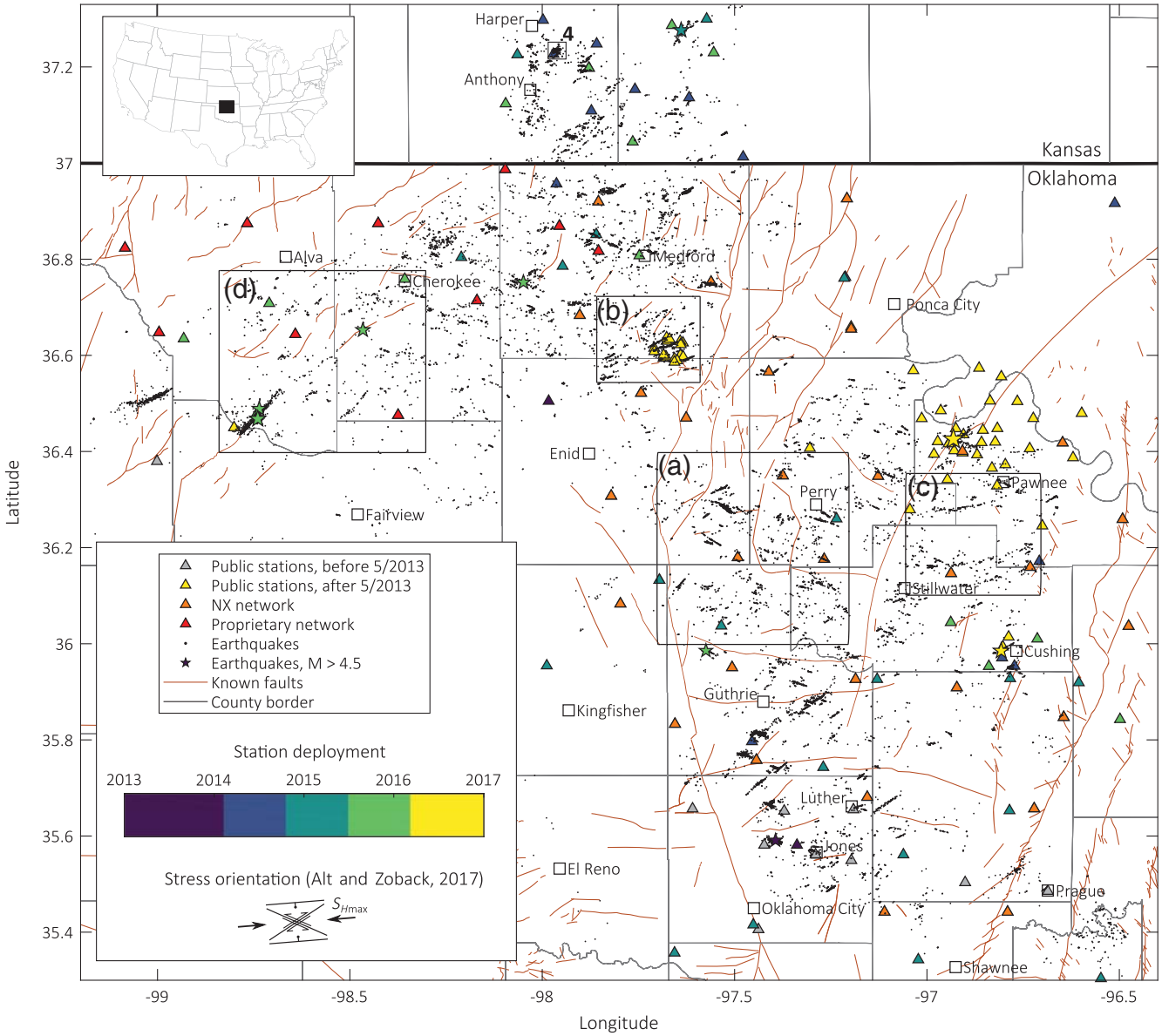

▲ **Figure 2.** Map of relocated earthquakes for the Oklahoma and southern Kansas area. (Inset) The location of the section in the United States. Black dots are earthquakes; stars mark earthquakes with $M \geq 4.5$. Triangles are seismic stations queried for the relocations with colors as follows: red marks stations of the proprietary network; orange are the NX network stations; gray are public stations that were installed before 31 May 2013 and were installed until at least March 2016. Other triangles are stations deployed later, with the deployment time color coded. The bold line marks the Oklahoma–Kansas border; thin lines are county borders. Brown lines are faults from Holland (2015). Rectangles mark close-ups in Figures 3 and 4. The orientation of the maximum horizontal stress from Alt and Zoback (2017), along with critically stressed fault orientations, is indicated in the legend.

Depths

Depths are referred relative to the ground surface, which is about 300 m above sea level throughout the region. In Figure 5, we plot a histogram of earthquake depths relative to the basement depth for earthquakes that have an absolute uncertainty in depth < 1 km. Basement depth was obtained from a data set of wells that reach the basement (Campbell and Weber, 2006). This data set was interpolated using Kriging to get the basement depth at the earthquake epicenters. Generally, the top of basement varies smoothly between 1 and 2 km below the ground surface. From the distribution, it is seen that almost all earthquakes occur in the basement, with the mean and mode values of 4.0 and 4.5 km below top of basement, respectively (Fig. 5).

At closer inspection, we notice that, for earthquake clusters more than about one focal depth away from the nearest stations, we lose depth resolution. For faults illuminated by hypocenters distributed in a dipping plane, the relative depth distribution may get compressed; that is, the plane outlined by hypocenters appears to have a smaller dip than is mechanically

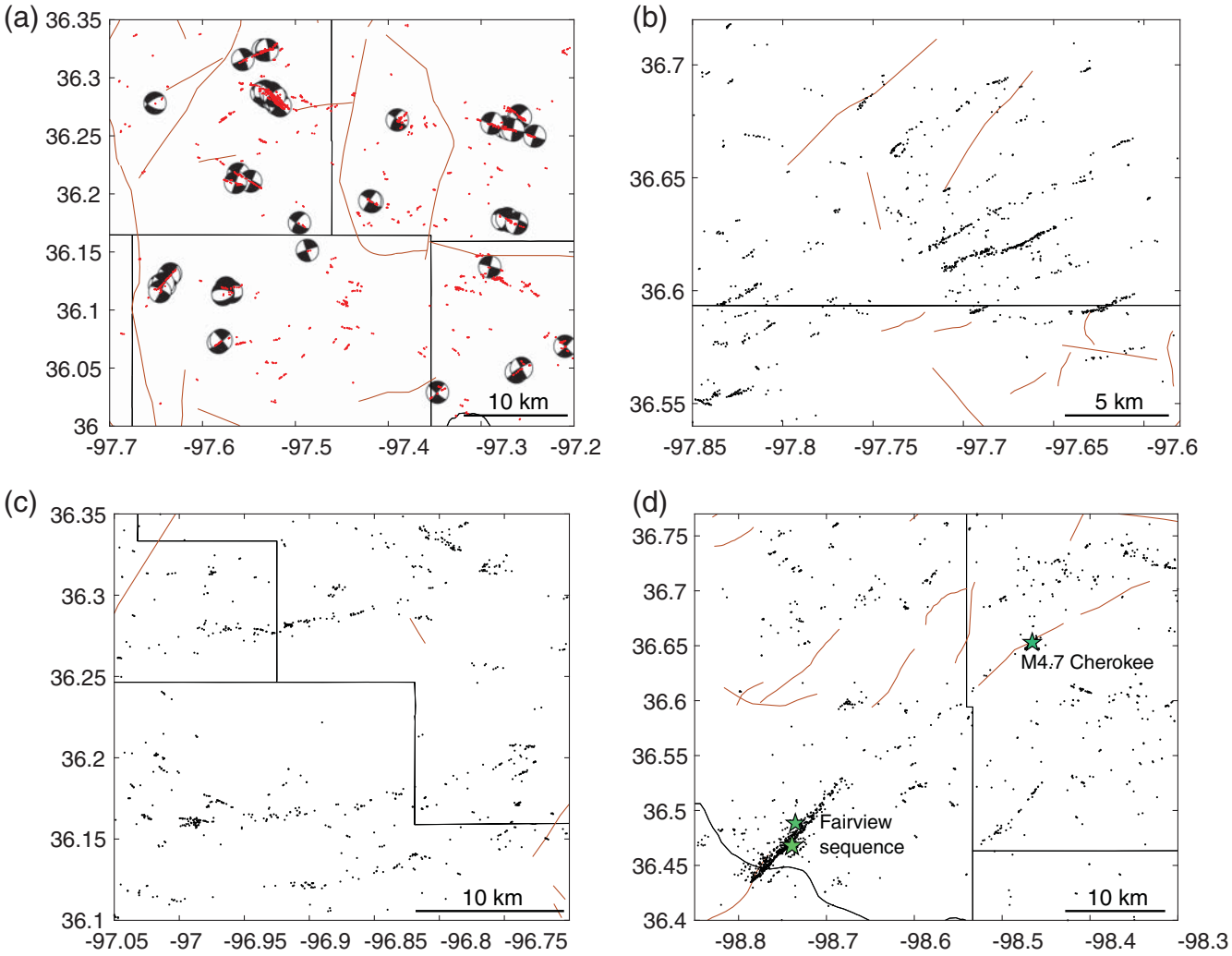

▲ **Figure 3.** Close-ups of Figure 2. (a) A comparison to moment-tensor solutions (courtesy of R. B. Herrmann, see description in Herrmann *et al.*, 2011). Only events relocated with waveform cross correlation are drawn. (b) A set of subparallel faults, (c) three east–west arcs of potential en echelon fault zones, and (d) the Fairview and Cherokee sequences with a potential lineament connecting both sequences and known fault segments.

reasonable. For subvertical faults, this may lead to hypocenters merely forming a string of earthquakes rather than a plane. This problem is exaggerated because of the relatively shallow depth of about 5 km for these earthquakes. This highlights the need for seismic monitoring networks with tight station spacing to adequately monitor relatively shallow-induced seismicity.

Here, we stress that absolute depths are highly dependent on the chosen velocity model. We tested a variety of reasonable velocity models, and in each case the vast majority of earthquake hypocenters remain several kilometers below the Arbuckle-basement contact.

CONCLUSIONS

We present a new catalog of relocated earthquakes for the Oklahoma–Kansas area covering the period from May 2013 to November 2016. Within this period, we cover the major increase of seismicity in the region. We are missing, however, the initiation phase of the induced seismicity crisis beginning in about 2009 and including the 2011 M 5.7 Prague earthquake and aftershock sequence. We improve absolute location precision by more than one order of magnitude compared to previously available data sets. Relative locations reduce the scatter by another order of magnitude, resolving the local fault geometry. Earthquakes align on predominantly subvertical faults, with reactivated extent of up to 20 km and possibly up to 50 km. Our catalog enables detailed studies of the evolution of earthquake sequences and of the fault structures in the region.

The catalog can be found in the Ⓔ electronic supplement to this article.

DATA AND RESOURCES

The National Earthquake Information Center (NEIC) provides earthquake data and phase information at http://earthquake.usgs.gov/earthquakes/search/ (last accessed No-

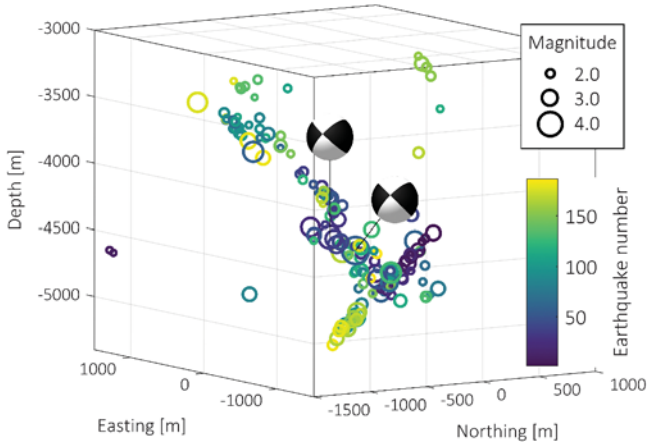

▲ **Figure 4.** A set of two normal faults between Harper and Anthony, Kansas. Moment tensors (courtesy of R. B. Herrmann) of the largest two events (*M* 4.3 and *M* 3.8, respectively) are in excellent agreement with the fault planes resolved from hypocenters. Earthquakes are colored in order of occurrence and scaled by magnitude.

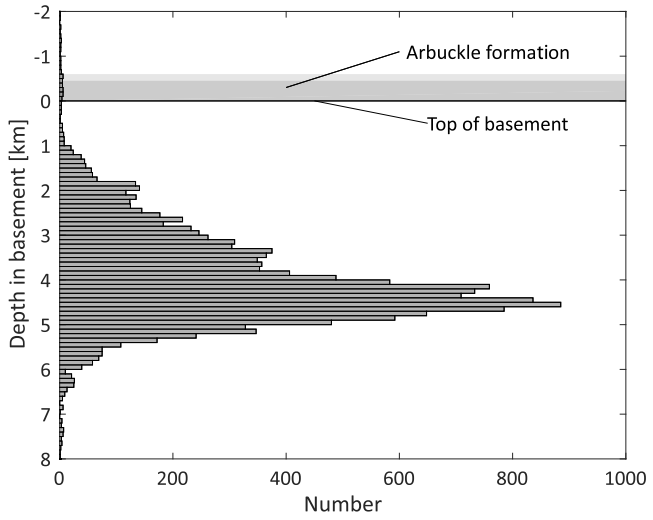

▲ **Figure 5.** Distribution of earthquake depth relative to the top of basement. Basement depth was interpolated using Kriging from Campbell and Weber (2006). Gray patches mark the approximate depth interval of the Arbuckle group.

vember 2016). The Oklahoma Geological Survey earthquake catalog can be found at http://www.ou.edu/content/ogs/research/earthquakes/catalogs.html (last accessed November 2016). Most waveform data are available from Incorporated Research Institutions for Seismology Data Management Center (IRIS–DMC) including one company-operated network (network code NX). Additional waveform data were provided by sponsors of the Stanford Center for Induced and Triggered Seismicity. Moment tensors can be downloaded from http://www.eas.slu.edu/eqc/eqc_mt/MECH.NA/index.html (last accessed November 2016).

ACKNOWLEDGMENTS

M. S. acknowledges support by the Alexander von Humboldt Foundation. Both authors were supported by the Stanford Center for Induced and Triggered Seismicity. The authors acknowledge thoughtful reviews by Patricia Martínez-Garzón, Ryan Schulz, and an Associate Editor that considerably helped to improve the article.

REFERENCES

Alt, R. C., and M. D. Zoback (2017). In situ stress and active faulting in Oklahoma, *Bull. Seismol. Soc. Am.* **107,** no. 1, 216–228, doi: 10.1785/0120160156.

Campbell, J. A., and J. L. Weber (2006). *Wells Drilled to Basement in Oklahoma*, Oklahoma Geological Survey, Norman, Oklahoma, Special Publication, 2006-1.

Chen, C., and A. A. Holland (2016). PhasePApy: A robust pure Python package for automatic identification of seismic phases, *Seismol. Res. Lett.* **87,** no. 6, 1384–1396, doi: 10.1785/0220160019.

Chen, X., P. M. Shearer, and R. E. Abercrombie (2012). Spatial migration of earthquakes within seismic clusters in southern California: Evidence for fluid diffusion, *J. Geophys. Res.* **117,** no. 4, 1–7, doi: 10.1029/2011JB008973.

Darold, A. P., A. A. Holland, J. K. Morris, and A. R. Gibons (2015). Oklahoma earthquake summary report 2014, *Okla. Geol. Surv. Open-File Rept. OF1-2015*.

Deichmann, N., and M. Garcia-Fernandez (1992). Rupture geometry from high-precision relative hypocentre locations of microearthquake clusters, *Geophys. J. Int.* **110,** no. 3, 501–517, doi: 10.1111/j.1365-246X.1992.tb02088.x.

Ellsworth, W. L. (2013). Injection-induced earthquakes, *Science* **341,** no. 6142, 1,225,942–1,225,942, doi: 10.1126/science.1225942.

Hauksson, E., J. Stock, R. Bilham, M. Boese, X. Chen, E. J. Fielding, J. Galetzka, K. W. Hudnut, K. Hutton, L. M. Jones, *et al.* (2013). Report on the August 2012 Brawley earthquake swarm in Imperial Valley, southern California, *Seismol. Res. Lett.* **84,** no. 2, 177–189, doi: 10.1785/0220120169.

Herrmann, R. B., H. Benz, and C. J. Ammon (2011). Monitoring the earthquake source process in North America, *Bull. Seismol. Soc. Am.* **101,** no. 6, 2609–2625, doi: 10.1785/0120110095.

Holland, A. A. (2015). Preliminary fault map of Oklahoma, *Okla. Geol. Surv. Open-File Rept. OF3-2015*.

Klein, F. W. (2014). User's guide to HYPOINVERSE-2000, a Fortran program to solve for earthquake locations and magnitude, *U.S. Geol. Surv. Open-File Rept. 02-171*, revised June 2014.

Krischer, L., T. Megies, R. Barsch, M. Beyreuther, T. Lecocq, C. Caudron, and J. Wassermann (2015). ObsPy: A bridge for seismology into the scientific Python ecosystem, *Comput. Sci. Discov.* **8,** no. 1, 14003, doi: 10.1088/1749-4699/8/1/014003.

Maeda, N. (1985). A method for reading and checking phase time in auto-processing system of seismic wave data, *Zisin* **38,** no. 3, 365–379, doi: 10.4294/zisin1948.38.3_365.

Raleigh, C. B., J. H. Healy, and J. D. Bredehoeft (1976). An experiment in earthquake control at Rangely, Colorado, *Science* **191,** no. 4233, 1230–1237, doi: 10.1126/science.191.4233.1230.

Schoenball, M., N. C. Davatzes, and J. M. G. Glen (2015). Differentiating induced and natural seismicity using space-time-magnitude statistics applied to the Coso Geothermal field, *Geophys. Res. Lett.* **42,** no. 15, 6221–6228, doi: 10.1002/2015GL064772.

Shelly, D. R., W. L. Ellsworth, and D. P. Hill (2016). Fluid-faulting evolution in high definition: Connecting fault structure and frequency–magnitude variations during the 2014 Long Valley Caldera, California, earthquake swarm, *J. Geophys. Res.* **121,** no. 3, 1776–1795, doi: 10.1002/2015JB012719.

Vidale, J. E., and P. M. Shearer (2006). A survey of 71 earthquake bursts across southern California: Exploring the role of pore fluid pressure fluctuations and aseismic slip as drivers, *J. Geophys. Res.* **111,** no. B5, B05312, doi: 10.1029/2005JB004034.

Waldhauser, F., and W. L. Ellsworth (2000). A double-difference earthquake location algorithm: Method and application to the northern Hayward fault, California, *Bull. Seismol. Soc. Am.* **90,** no. 6, 1353–1368, doi: 10.1785/0120000006.

Walsh, F. R., and M. D. Zoback (2015). Oklahoma's recent earthquakes and saltwater disposal, *Sci. Adv.* **1,** no. 5, e1500195–e1500195, doi: 10.1126/sciadv.1500195.

Walsh, F. R., and M. D. Zoback (2016). Probabilistic assessment of potential fault slip related to injection-induced earthquakes: Application to north-central Oklahoma, USA, *Geology* **44,** no. 12, 991–994, doi: 10.1130/G38275.1.

Weingarten, M., S. Ge, J. W. Godt, B. A. Bekins, and J. L. Rubinstein (2015). High-rate injection is associated with the increase in U.S. mid-continent seismicity, *Science* **348,** no. 6241, 1336–1340.

Yeck, W. L., M. Weingarten, H. M. Benz, D. E. McNamara, E. A. Bergman, R. B. Herrmann, J. L. Rubinstein, and P. S. Earle (2016). Far-field pressurization likely caused one of the largest injection induced earthquakes by reactivating a large preexisting basement fault structure, *Geophys. Res. Lett.* **43,** no. 19, 10,198–10,207, doi: 10.1002/2016GL070861.

Zaliapin, I., and Y. Ben-Zion (2013). Earthquake clusters in southern California I: Identification and stability, *J. Geophys. Res.* **118,** no. 6, 2847–2864, doi: 10.1002/jgrb.50179.

Zaliapin, I., and Y. Ben-Zion (2016). Discriminating characteristics of tectonic and human-induced seismicity, *Bull. Seismol. Soc. Am.* **106,** no. 3, 846–859, doi: 10.1785/0120150211.

Martin Schoenball
William L. Ellsworth
Department of Geophysics
Stanford University
397 Panama Mall
Stanford, California 94305-2215 U.S.A.
schoenball@stanford.edu
wellsworth@stanford.edu

Published Online 5 July 2017